Quantum Electronics **38** (6) 570 – 575 (2008)

PACS numbers: 42.30.Wb; 87.63.L–; 87.64.Cc; 87.55.K–
DOI: 10.1070/QE2008v038n06ABEH013842

Role of multiple scattering in formation of OCT skin images

M.Yu. Kirillin, A.V. Priezzhev, R. Myllylä

Abstract. **Optical coherence tomography (OCT) images of model human skin samples are obtained by using Monte Carlo simulations. The contributions of least and multiple scattering, diffusion and nondiffusion components and of separate scattering orders are studied by using a multilayer skin model based on experimental images. The model images are obtained by neglecting speckles or taking them into account. It is shown that least scattering forms the image of the upper skin layers, while the contribution of multiple scattering can be characterised as a blurred full image with a lower contrast. Repeated scattering mainly contributes to the OCT image at depths up to 1 mm. The diffusion component contributes to the image beginning from the epidermal basal layer. The partial image produced by this component is more blurred compared to the partial image produced by to multiple scattering. The nondiffusion component forms the OCT skin image at depths up to ~ 1.3 mm.**

Keywords: *optical coherence tomography, Monte Carlo simulations, multiple scattering, skin structure visualisation.*

1. Introduction

The method of optical coherence tomography (OCT) was first introduced in 1991 [1] and at present OCT is one of the most promising methods for noninvasive diagnostics of optically inhomogeneous media. Being based on the principles of low-coherence interferometry, OCT allows the reconstruction of the in-depth distribution of optical properties in an object from the interference pattern produced upon the interference between radiation backscattered from the object under study located in the sample arm of a Michelson interferometer and radiation reflected from a mirror in the reference arm of the interferometer [2].

One of the most actual biomedical applications of OCT is noninvasive imaging of the internal structure of upper skin layers [3], which is very important for early detection of skin cancer. The obtained images are characterised by a high resolution (a few microns). However, skin is a highly scattering medium in the NIR range, where the probing is usually performed. As a result, the depth of undistorted imaging in skin is limited by the contribution of multiple scattering, which increases with increasing the probing depth.

The effect of multiple scattering on the formation of the OCT images of highly scattering media can be reduced by various methods. However, it is impossible to eliminate this effect completely by hardware means. In addition, the problem is complicated by the fact that the radiation transfer equation describing light propagation in a scattering medium [4, 5] has no general analytical solution, whereas the field of application of approximate solutions is significantly limited. In these circumstances, the Monte Carlo (MC) method of numerical statistical simulations providing possibilities for identification and classification of photons contributing to the OCT image is a convenient and efficient tool for analysis of the role of multiple scattering in the OCT image formation.

Along with advantages such as noninvasiveness and a high spatial resolution, the OCT technique also has several disadvantages related to the peculiarities of signal formation. On the one hand, the OCT signal is produced due to the interference between the waves reflected from the reference mirror and backscattered from the sample. On the other hand, the backscattered waves can interfere with each other producing speckles that decrease the OCT image quality [6].

Speckles appear due to the interference of coherent waves reflected from a random inhomogeneous medium. Apart from the structure and optical properties of an object and its movement, the parameters of speckles depend on the parameters of probe radiation, the character of scattering and phase aberrations of radiation propagating in the medium and on the detector aperture.

Skin is a multilayer structure and the optical properties of various skin layers are different. Therefore, to describe adequately the propagation of light in skin, it is necessary either to specify the optical properties of individual layers or to use effective optical parameters characterising skin as a whole rather than the properties of individual layers. However, when the specific features of the layered structure

A.V. Priezzhev Department of Physics, M.V. Lomonosov Moscow State University, Vorob'evy Gory, 119992 Moscow, Russia;
e-mail: avp2@mail.ru;
M.Yu. Kirillin University of Oulu, Optoelectronics and Measurement Techniques Laboratory, P.O. Box 4500, 90014 University of Oulu, Oulu, Finland; Department of Physics, M.V. Lomonosov Moscow State University, Vorob'evy Gory, 119992 Moscow, Russia;
e-mail: mkirillin@yandex.ru;
R. Myllylä University of Oulu, Optoelectronics and Measurement Techniques Laboratory, P.O. Box 4500, 90014 University of Oulu, Oulu, Finland; e-mail: risto.myllyla@ee.oulu.fi

Received 24 December 2007; revision received 13 March 2008
Kvantovaya Elektronika **38** (6) 570 – 575 (2008)
Translated by M.Yu. Kirillin

of skin are important, the efficient parameters cannot be used. In addition, it should be taken into account that the optical parameters of skin *in vivo* and *in vitro* are considerably different.

The optical properties of skin can be measured by various methods [7–11]. The parameters are reconstructed from experimental data by using, as a rule, the inverse MC method or theoretical calculations. However, the obtained results strongly depend on the applied technique. The method for determining the optical properties of skin from the OCT A-scan shape was first proposed in paper [12] and then refined in [13–16]. However, the values of the scattering coefficient obtained by this method differ by an order of magnitude from those obtained by other methods. For this reason, we used in our paper the scattering coefficients obtained by averaging the values measured by different methods.

The aim of this paper is to study the contributions of different scattering orders to the OCT image obtained by simulations performed for a six-layer skin model, and to separate the contributions of least and multiple scattering and of nondiffusion and diffusion components. Such analysis should provide the understanding of the OCT image formation, which is important for the development of the OCT image processing techniques for obtaining additional information.

2. Photon classification

In this paper, we use two classifications of photons contributing to the OCT image. The first one is related to the possibility of localisation of an object from which a photon was backscattered [17]. A photon is called a multiply scattered photon (MSP) if the difference between its optical pathlength l in a medium and its doubled maximum optical penetration depth $2z_{\max}$, in the medium exceeds the coherence length l_{coh} of the source:

$$l - 2z_{\max} > l_{\mathrm{coh}}. \tag{1}$$

In this case, it is assumed that the photon carries distorted information on the localisation depth of the scatterer. In the opposite case, photons carry reliable information on the localisation depth of the scatterer and are called least scattered photons (LSPs). Our preliminary studies showed that the calculation of the maximum optical depth based on the averaged layer thicknesses give incorrect results and, because of this, we calculated $z_{\max}$ separately for each photon taking into account the layer boundary relief in the photon propagation region.

According to the second classification based on the diffusion theory [18], a photon is assigned to the diffusion component if its optical pathlength l exceeds the mean transport length l_{tr} in the medium. In this case the photon 'forgets' its initial propagation direction in the medium. We will use a somewhat different definition based on the fact that the criterion for photon direction randomisation in a medium is the number of photon scattering events, rather than the path propagated by the photon. Thus, the photon belongs to the diffusion component photon (DCP) if the number N of photon scattering events exceeds the mean number N_{cr} of scattering events per transport length,

$$N > N_{\mathrm{cr}} = \frac{\mu_{\mathrm{a}} + \mu_{\mathrm{s}}}{\mu_{\mathrm{a}} + \mu'_{\mathrm{s}}}, \tag{2}$$

where $l_{\mathrm{tr}} = (\mu_{\mathrm{a}} + \mu'_{\mathrm{s}})^{-1}$ is the transport length; $\mu'_{\mathrm{s}} = \mu_{\mathrm{s}}(1-g)$ is the reduced scattering coefficient; $g = \langle \cos\theta \rangle$ (θ is the scattering angle) is the anisotropy factor; $l_{\mathrm{fp}} = (\mu_{\mathrm{a}} + \mu_{\mathrm{s}})^{-1}$ is the photon mean free path; μ_{a} and μ_{s} are the absorption and scattering coefficients, respectively. In the opposite case, the photon propagation direction is considered not random and photons belong to the nondiffusion component.

3. Monte Carlo simulations of OCT signals and images

Monte Carlo simulations are based on the calculation of a large number of random photon trajectories in a scattering medium [19]. The optical properties of the medium (scattering and absorption coefficients, phase function or anisotropy factor, refractive index) determine the lengths and shapes of individual photon trajectories. In this paper, we use the program code of the MC algorithm developed earlier in [20, 21] to simulate OCT signals. Simulations were performed by using the Henyey–Greenstein phase function, which is widely applied for MC simulations of light propagation in biotissues, in particular, skin [22]:

$$f_{\mathrm{HG}}(\theta) = \frac{1}{4\pi} \frac{1 - g^2}{(1 + g^2 - 2g\cos\theta)^{3/2}}. \tag{3}$$

An OCT signal from an optically inhomogeneous object is a superposition of fringe patterns formed by interference of low-coherent radiation backscattered from the object and the reference radiation. The signal structure is determined by the inhomogeneous distribution of optical properties inside the object. The OCT signal is simulated by calculating the optical paths of photons in the object and reference arms and calculating then their optical mixing. We assume that the coherence function has a Gaussian shape. Each in-depth scan (A-scan) was simulated by using 5 millions of weighted photons.

The light intensity in the measurement arm of the interferometer is decribed by the expression [23]

$$I(\tau) = \langle [E_{\mathrm{r}}(t) + E_{\mathrm{s}}(t+\tau)]^2 \rangle = I_{\mathrm{r}} + I_{\mathrm{s}} + 2\sqrt{I_{\mathrm{r}} I_{\mathrm{s}}} \mathrm{Re} C(\tau), \tag{4}$$

where E_{r}, E_{s} and I_{r} and I_{s} are the amplitudes and intensities of the waves coming from the reference and object arms, respectively; the angle brackets denote averaging over t;

$$C(\tau) = \langle E_{\mathrm{r}}(t) + E_{\mathrm{s}}^*(t+\tau) \rangle / \sqrt{I_{\mathrm{r}} I_{\mathrm{s}}} \tag{5}$$

is the normalised coherence function. For a narrow frequency interval $\Delta\nu/\langle\nu\rangle \ll 1$ and small values of τ ($\Delta\nu\tau \ll 1$), expression (4) can be written in the form

$$I(\tau) = I_{\mathrm{r}} + I_{\mathrm{s}} + 2\sqrt{I_{\mathrm{r}} I_{\mathrm{s}}} |C(\tau)| \cos(2\pi\langle\nu\rangle\tau), \tag{6}$$

where $|C(\tau)|$ is the degree of the time coherence of radiation. In the absence of dispersion in the medium, function (5) coincides with the source coherence function:

$$C(\tau) = \langle E(t) E^*(t+\tau) \rangle / \langle E(t) E^*(t) \rangle. \tag{7}$$

The intensities I_{r} and I_{s} in (6) are independent of the reference mirror position and form the constant component of the detected signal, whereas the interference term changes with the movement of the reference mirror and

carries information on the distribution of the optical properties of the object over depth.

By using expressions (4)–(7), the output OCT signal was calculated from the distribution of the detected photons over the optical paths [20]:

$$I(t) = \sum_i \sqrt{N_r N_s(t, \Delta l_i)} \cos\left(\frac{2\pi}{\lambda}\Delta l_i\right) \exp\left[-\left(\frac{\Delta l_i}{l_{coh}}\right)^2\right], \quad (8)$$

where $N_r(t, \Delta l_i)$ and $N_s(t, \Delta l_i)$ are the numbers of detected photons coming from the reference and object arms, respectively; Δl_i is the path difference; and l_{coh} is the coherence length of the probe radiation. The exponential term in (8) determines the Gaussian shape of the coherence function. Note that expression (8) accounts for the so-called speckle structure produced by the overlap of interference patterns. Speckles can be eliminated by different methods (for example, spatial averaging over several A-scans) [2]. The elimination of speckles in simulations can be combined with the calculation of the signal envelope by using the expression

$$I(t) = \sum_i \sqrt{N_r N_s(t, \Delta l_i)} \exp\left[-\left(\frac{\Delta l_i}{l_{coh}}\right)^2\right] \quad (9)$$

instead of (8).

The OCT images are obtained by calculating successive A-scans by displacing the point of incidence of probe radiation with a specified step along a selected direction. The total number of A-scans and the step between them are preliminary specified. The step is usually chosen equal to the probe beam diameter (FWHM). The OCT images can be calculated taking speckles into account or neglecting them.

The OCT images of a multilayer human skin phantom were simulated for the probe radiation wavelength of 910 nm and $l_{coh} = 10$ μm as in the setup used in [24]. A two-dimensional OCT image was simulated by calculating 50 A-scans with a transversal step of 20 μm. The typical calculation time of an OCT image of human skin was about 10 hours by using an AMD Athlon™ 3000 PC.

4. Multilayer skin model

The experimental OCT image of human skin (thick skin of a young male thumb) presented in Fig. 1a was used as a base for constructing a multilayer skin model used in our simulations. Figure 1a demonstrates distinctly skin layers, which were used in simulations (scheme in Fig. 1b). The thickness and shape of the lower skin layers were chosen according to the parameters of the skin structure presented in [22].

The optical properties and typical thicknesses of various skin layers used in simulations are presented in Table 1. These values are obtained by averaging the data taken from [13, 22, 25].

Table 1. Optical properties of skin layers ($\lambda = 910$ nm).

Skin layer	Thickness/mm	μ_s/mm^{-1}	μ_s/mm^{-1}	g	n
Stratum corneum	0.02	40	0.02	0.9	1.54
Epidermis (prickle layer)	0.18	5	0.015	0.95	1.34
Epidermis (basal layer)	0.2	10	0.02	0.85	1.4
Dermis with upper plexus	0.2	10	0.1	0.9	1.39
Dermis	0.8	7	0.7	0.87	1.4
Dermis with lower plexus	0.6	12	0.2	0.95	1.39

5. Results and discussion

The model OCT images of skin calculated by neglecting speckles and taking them into account are shown in Fig. 2. One can see that these images demonstrate different skin layers, in accordance with experimental results presented in Fig. 1a. The consideration of speckles in the calculation of the OCT image introduces intense noise. This occurs due to the overlap of the fringe patterns and results in a decrease in the image contrast, although, the main details of the image calculated by neglecting speckles are also observed in the image calculated taking speckles into account.

Figure 3 presents contributions of LSPs and MSPs to the OCT image of skin calculated by neglecting speckles. One can see that the LSPs form mainly the image of the upper skin layers up to optical depths ~ 1 mm. The OCT image with the MSP contribution repeats in general the full OCT image (Fig. 2a), being, however, more blurred. This suggests that the main distortion introduced by MSP is the image blurring, rather than the image displacement to larger

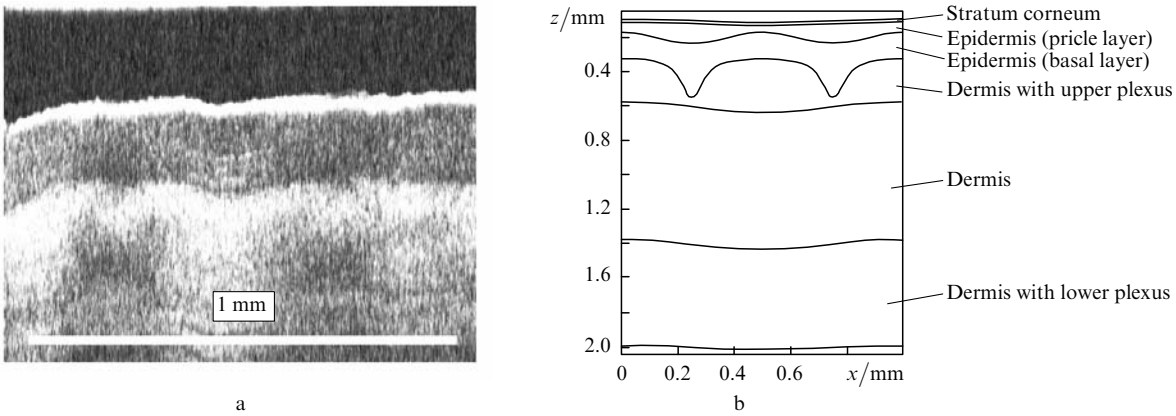

Figure 1. Experimental OCT image of human skin (a) and corresponding multilayer model (b).

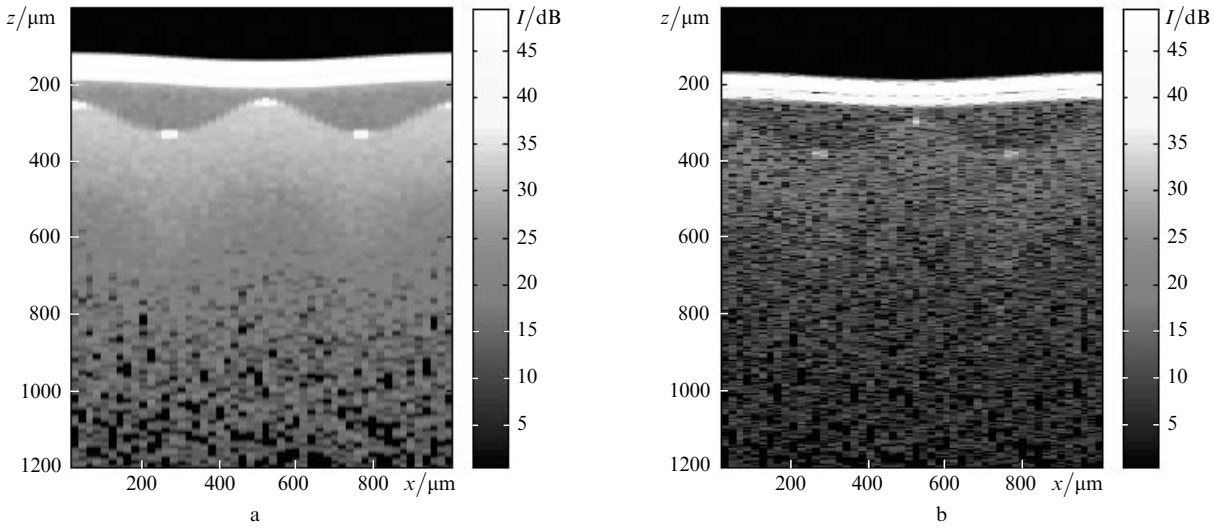

Figure 2. Simulated OCT images of skin without (a) and with (b) speckles of the signal.

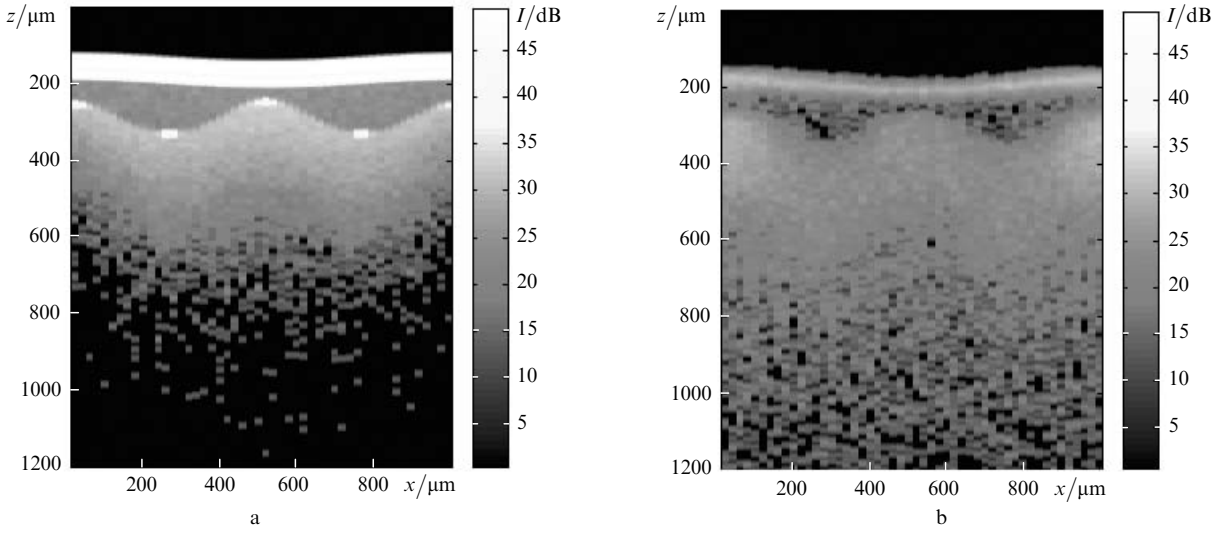

Figure 3. Contributions of least (a) and multiple (b) scattering to the OCT image of skin.

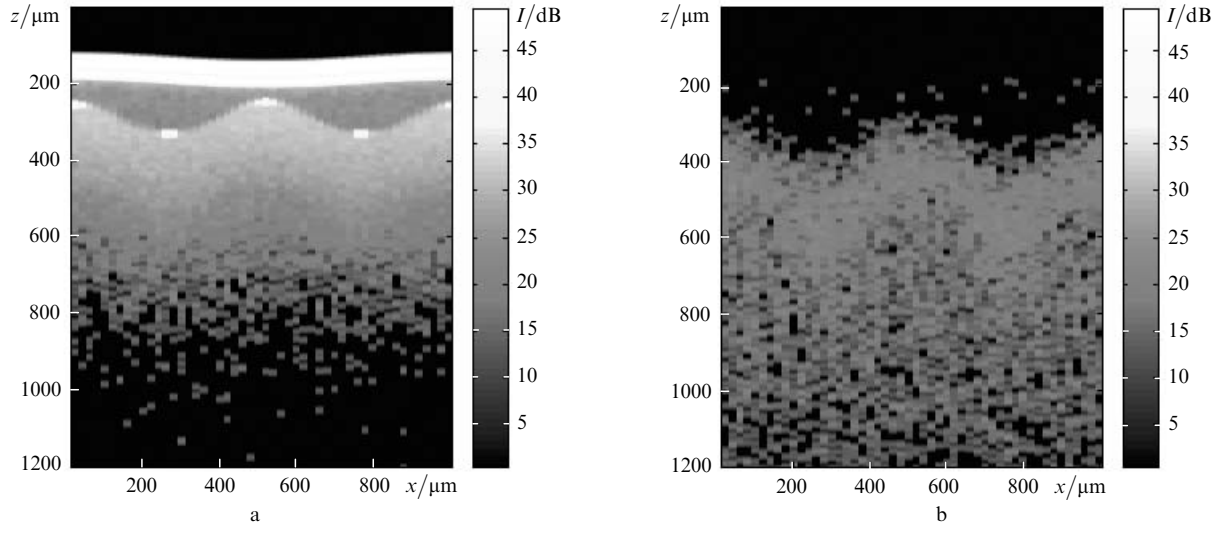

Figure 4. Contributions of NDCP (a) and DCP (b) to the OCT image of skin.

depths, which could be supposed from the definition (1) of multiple scttering.

Figure 4 presents the contributions of nondiffusion and diffusion components to the OCT image of skin calculated by neglecting speckles. One can see that the diffusion component contributes primarily to the imaging of deep skin layers and, producing as MSPs, a blurred OCT image; however, not of the whole sample, but only its lower layers. The image contrast in this case is lower than the contrast of the image of the contribution of multiple scattering. The nondiffusion component, similarly to LSPs, forms the image of upper skin layers at optical depths up to ~ 1.4 mm.

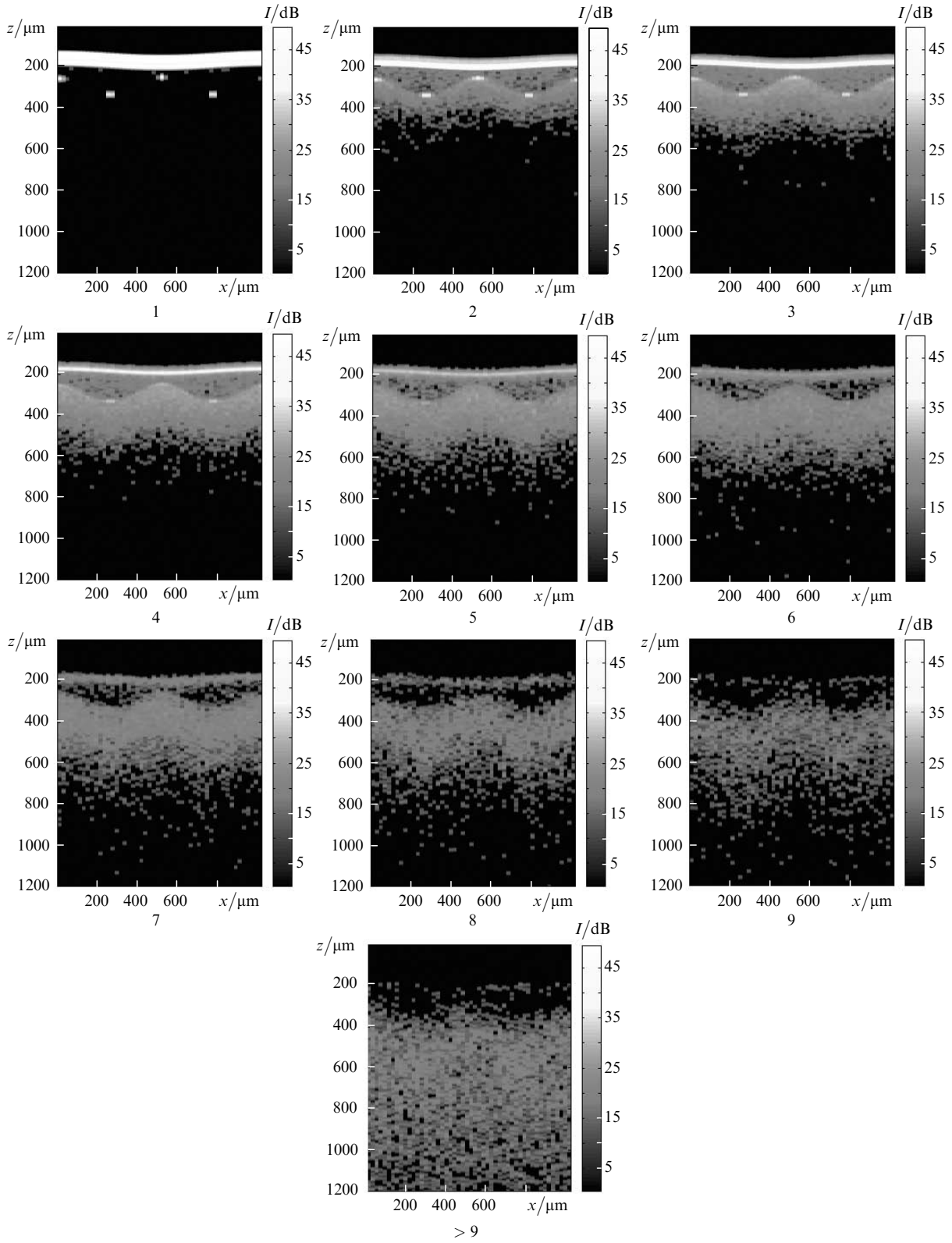

Figure 5. Contributions of different scattering orders to the OCT image of skin. The number of the image corresponds to the scattering order.

The contributions of individual scattering orders (from 1 to 9) to the OCT image of the skin sample considered above are shown in Fig. 5. Because the contributions of scattering orders above 9 are rather small and do not play a significant role in imaging of upper skin layers, Fig. 5 presents only their total contribution. Note, however, that each scattering order forms a partial image containing the main features of the total OCT image determined by the object geometry. The differences are mainly manifested in the signal level and contrast.

The first scattering order provides the imaging of the upper sample layer, the lower boundary of corneus layer and the parts of the boundary between epidermal layers that are perpendicular to the probing radiation direction. The second scattering order forms the image of the three upper layers of the considered skin sample. All the considered scattering orders contribute to the imaging of these layers, however, starting from the third scattering order, the contribution to the upper three layers decreases while the contribution to the imaging of the lower layers of the sample increases.

6. Conclusions

In this study we have obtained simulated OCT images of a skin sample with and without speckles by using the developed technique based on the Monte-Carlo simulations. The skin model was chosen based on the experimental data. The contribution of the different scattering orders and photon fractions to the obtained OCT image were distinguished. The separation of the contributing photons to least and multiply scattering components as well as to diffusive and nondiffusive components allowed their roles in the formation of OCT images to be analysed.

It has been shown that least scattering and nondiffusive components contribute to the OCT image of skin to optical depths about 1.2 mm. The partial image formed by multiple scattering exhibits the essential features of the full image, however, is more blurred. The effect of image shift to the larger depths due to elongation of the trajectories is negligible. The partial image formed by the diffusive component also repeats the essential features of the full image, however it is less contrasted compared to that of multiple scattering and exhibits almost no contribution to the upper three layers of the image. Analysis of the contribution of separate scattering orders showed that each scattering order forms the image featuring the essential details of the full OCT image, however, these partial images differ in the signal level and contrast.

Acknowledgements. This work was supported by the GETA Graduate School (Finland) and Tauno Tonning Foundation (Finland).

References

1. Huang D., Swanson E.A., Lin C.P., et al. *Science*, **254**, 1178 (1991).
2. Bouma B.E., Tearney G.J. (Eds) *Handbook of Optical Coherence Tomography* (New York: Marcel Dekker, 2002).
3. Steiner R., Kunzi-Rapp K., Scharffetter-Kochanek K. *Med. Laser Appl.*, **18**, 249 (2003).
4. Ishimaru A. *Electromagnetic Wave Propagation, Radiation, and Scattering* (New Jersey: Prentice Hall, 1991).
5. Kravtsov Yu.A, Orlov Yu.I. *Geometricheskaya optika neodnorodnyh sred* (Geometrical Optics of Turbid Media) (Moscow: Nauka, 1980).
6. Schmitt J.M., Xiang S.H., Yung K.M. *J. Biomed. Opt.,* **4**, 95 (1999).
7. Torricelli A., Pifferi A., Taroni P., et al. *Phys. Med. Biol.*, **46**, 2227 (2001).
8. Simpson C.R., Kohl M., Essenpreis M., Cope M. *Phys. Med. Biol.*, **43**, 2465 (1998).
9. Salomatina E., Jiang B., Novak J., Yaroslavsky A.N. *J. Biomed. Opt.*, **11**, 064026 (2006).
10. Matcher S.J., Cope M., Delpy D.T. *Appl. Opt.*, **36**, 386 (1997).
11. Bashkatov A.N., Genina E.A., Kochubey V.I., Tuchin V.V. *J. Phys. D: Appl. Phys.*, **38**, 2543 (2005).
12. Schmitt J.M., Knuttel A., Bonner R.F. *Appl. Opt.*, **32**, 6032 (1993).
13. Knuttel A., Boehlau-Godau M. *J. Biomed. Opt.*, **5**, 83 (2000).
14. Levitz D., Thrane L., Frosz M.H., et al. *Opt. Express*, **12**, 249 (2004).
15. Knüttel A., Bonev S., Knaak W. *J. Biomed. Opt.*, **9**, 265 (2004).
16. Kholodnykh A.I., Petrova I.Y., Larin K.V., et al. *Appl. Opt.*, **42**, 3027 (2003).
17. Wang R.K. *Phys. Med. Biol.*, **47**, 2281 (2002).
18. Kirillin M.Yu., Priezzhev A.V. *Kvantovaya Elektron.*, **32**, 883 (2002) [*Quantum Electron.*, **32**, 883 (2002)].
19. Wang L., Jacques S.L., Zheng L. *Comp. Meth. Progr. Biomed.,* **47**, 131 (1995).
20. Kirillin M.Yu., Meglinski I.V., Priezzhev A.V. *Kvantovaya Elektron.*, **36**, 247 (2006) [*Quantum Electron.*, **36**, 247 (2006)].
21. Kirillin M.Yu., Priezzhev A.V., Tuchin V.V., et al. *J. Phys. D: Appl. Phys.*, **38**, 2582 (2005).
22. Tuchin V.V. *Tissue Optics: Light Scattering Methods and Instruments for Medical Diagnosis* (Bellingham: SPIE Press, 2000).
23. Gurov I.P., in *Problemy nelineynoy i kogerentnoy optiki* (Problems of Nonlinear and Coherent Optics) (St. Petersburg, 2004) pp 6–30.
24. Kirillin M.Yu., Alarousu E., Fabritius T., Myllylä R., Priezzhev A.V. *J. Europ. Opt. Soc.–Rapid Publ.*, **2**, 07031 (2007).
25. Meglinski I.V., Matcher S.J. *Physiol. Meas.*, **23**, 741 (2002).